Small extracellular vesicles convey the stress response of tumour cells

PhD Thesis

Mária Harmati

Supervisor:

Krisztina Buzás, PhD

Faculty of Dentistry, University of Szeged

Biological Research Centre

Doctoral School of Interdisciplinary Medicine,

Faculty of Medicine, University of Szeged

Szeged

2019

The dissertation is based on the following publications:

I. **Harmati M**, Tarnai Z, Decsi G, Kormondi S, Szegletes Z, Janovak L, Dekany I, Saydam O, Gyukity-Sebestyen E, Dobra G, Nagy I, Nagy K, Buzas K. Stressors alter intercellular communication and exosome profile of nasopharyngeal carcinoma cells. *J Oral Pathol Med.* **46,** 259-266, DOI: https://doi.org/10.1111/jop.12486 (2017).

IF: 2.237; Q2

II. **Harmati M**, Gyukity-Sebestyen E, Dobra G, Janovak L, Dekany I, Saydam O, Hunyadi-Gulyas E, Nagy I, Farkas A, Pankotai T, Ujfaludi Zs, Horvath P, Piccinini F, Kovacs M, Biro T, Buzas K. Small extracellular vesicles convey the stress-induced adaptive responses of melanoma cells. *Sci Rep.* **9,** 15329; DOI: https://doi.org/10.1038/s41598-019-51778-6 (2019).

Estimated IF: 4.011; Q1

Other full papers published during the PhD fellowship:

III. Buzas K, Marton A, Vizler C, Gyukity-Sebestyen E, **Harmati M**, Nagy K, Zvara A, Katona RL, Tubak V, Endresz V, Nemeth IB, Olah J, Vigh L, Biro T, Kemeny L. Bacterial sepsis increases survival in metastatic melanoma: *Chlamydophila pneumoniae* induces macrophage polarization and tumor regression. *J. Invest. Dermatol.* **136,** 862-865. DOI: https://doi.org/10.1016/j.jid.2015.12.032 (2016)

IF 6.287; Q1

IV. **Harmati M**, Gyukity-Sebestyen E, Dobra G, Terhes G, Urban E, Decsi G, Mimica-Dukic N, Lesjak M, Simin N, Pap B, Nemeth IB, Buzas K. Binary mixture of *Satureja hortensis* and *Origanum vulgare subsp. hirtum* essential oils: *in vivo* therapeutic efficiency against *Helicobacter pylori* infection. *Helicobacter.* **22,** e12350; DOI: https://doi.org/10.1111/hel.12350 (2017).

IF 4.123; Q1

V. Zsedenyi A, Farkas B, Abdelrasoul GN, Romano I, Gyukity-Sebestyen E, Nagy K, **Harmati M**, Dobra G, Kormondi S, Decsi G, Nemeth IB, Diaspro A, Brandi F, Beke S, Buzas K. Gold nanoparticle-filled biodegradable photopolymer scaffolds induced muscle remodeling: *in vitro* and *in vivo* findings. *Mater Sci Eng C Mater Biol Appl*. **72,** 625-630. DOI: https://doi.org/10.1016/j.msec.2016.11.124 (2017)

IF 5.080; Q1

VI. Decsi G, Soki J, Pap B, Dobra G, **Harmati M**, Kormondi S, Pankotai T, Braunitzer G, Minarovits J, Sonkodi I, Urban E, Nemeth IB, Nagy K, Buzas K. Chicken or the Egg: Microbial Alterations in Biopsy Samples of Patients with Oral Potentially Malignant Disorders. *Pathol Oncol Res.* **25,** 1023-1033. DOI: https://doi.org/10.1007/s12253-018-0457-x (2019).

Estimated IF 2.433; Q2

VII. Körmöndi S, Terhes G, Pal Z, Varga E, **Harmati M**, Buzas K, Urban E. Human Pasteurellosis Health Risk for Elderly Persons Living with Companion Animals. *Emerg Infect Dis.* **25,** 229-235. DOI: https://doi.org/10.3201/eid2502.180641 (2019).

Estimated IF 7.185; Q1

VIII. Gyukity-Sebestyen E, **Harmati M**, Dobra G, Nemeth I B, Mihaly J, Zvara Á, Hunyadi-Gulyas E, Katona R, Nagy I, Horvath P, Balind A, Szkalisity A, Kovacs M, Pankotai T, Borsos B, Erdelyi M, Szegletes Zs, Vereb Z, Buzas E I, Kemeny L, Biro T, Buzas K. Melanoma-Derived Exosomes Induce PD-1 Overexpression and Tumor Progression via Mesenchymal Stem Cell Oncogenic Reprogramming. *Front. Immunol.* **10,** 2459; DOI: https://doi.org/10.3389/fimmu.2019.02459 (2019).

Estimated IF: 4.716; Q1

Cumulative IF 36.072

1. Introduction

Extracellular vesicles (EVs) are lipid bound vesicles secreted by cells into the extracellular space. The three main types of EVs are microvesicles, apoptotic bodies and exosomes, which are differentiated based on their biogenesis, release pathway, size, content, and function. The smallest EVs are the exosomes (30-150 nm), which are formed within the endosomal network. In practice, the isolated material usually contains a mixture of EVs and consensus has not yet emerged on specific markers of EV subtypes. A guideline, called Minimal information for studies of extracellular vesicles 2018 (MISEV2018) suggests the use of operational terms for EV subtypes. Since we isolated EVs based on their size (<220 nm), here I refer to them as 'small EVs' (sEVs), even though their exosomal characteristics are demonstrated.

Exosomes play a critical role in the intercellular communication of adjacent as well as distal cells. They transfer lipids, proteins and a wide variety of genetic materials, such as DNA, mRNA, and non-coding RNAs. Inside the exosomal lipid bilayer, cytokines, miRNAs and other signalling molecules are protected from extracellular enzymes, ensuring that the exosomal cargo is delivered to the target cell in a functionally active form. In this way, exosomes are associated with numerous physiological and pathological conditions, including cancer diseases. Therefore, the exosome-mediated molecules and signalling pathways are of intense interest as potential diagnostic and therapeutic targets for personalised medicine.

Several recent papers have emphasized the mediating role of exosomes in tumorigenesis, tumour growth, metastasis and immune modulation at both local and distant malignant sites. They are not only involved in the paracrine communication in the tumour microenvironment, but as a systemic effect, exosomes participate in conditioning the secondary tumour sites as well (Fig.1). Upon contact with recipient cells, tumour-derived exosomes alter their phenotypic and functional properties conveying molecular and genetic messages.

As the existing vasculature of solid tumours cannot fulfill the increasing oxygen demand of rapidly expanding tumours, hypoxic and necrotic areas are formed. These areas have a special chemical microenvironment with low oxygen, low pH and low nutrient concentration, which increases the exosome release of malignant cells. Thus, content analysis of exosomes released under different stress conditions may reveal their function in tumour progression, and contribute to developing more efficient sEV-based strategies for cancer prognosis and therapy.

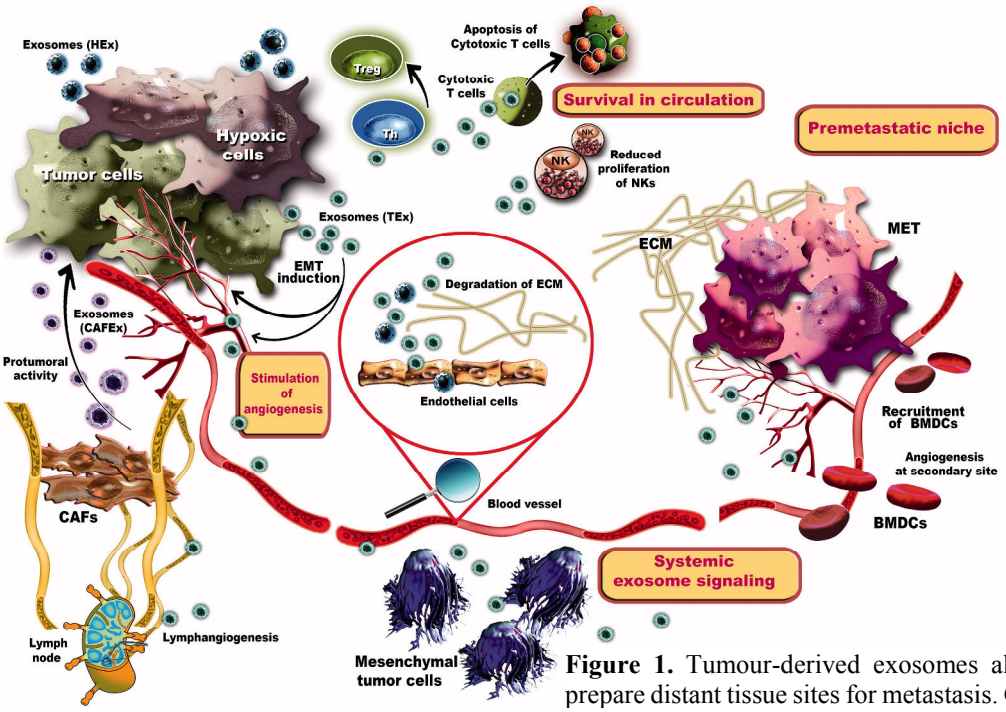

Figure 1. Tumour-derived exosomes alter the TME and prepare distant tissue sites for metastasis. Gulei *et al.* (2018).

2. Aims

In this study, we aimed to compare the vesicular information transfer of the 5-8F human nasopharyngeal carcinoma (NPC) and the B16F1 mouse melanoma cells under different microenvironmental conditions. We performed a comprehensive quantitative and qualitative comparison of the tumour-derived sEVs. Our specific aims were

1. to compare the sEV release under different microenvironmental conditions,
2. to describe the molecular pattern of sEV groups, which were released under various microenvironmental conditions,
3. to investigate potential doxorubicin and Ag-TiO_2 transfer by sEVs,
4. to establish an *in silico* model for the functional activity of sEVs in the recipient cells,
5. to compare functional properties of sEV groups, which were released under various microenvironmental conditions,
6. to compare the adaptivity of sEV-mediated communication of different tumour cells,
7. to describe the response patterns of sEV recipient cells, induced by the melanoma-derived sEV groups,
8. to compare the cellular migratory response to the melanoma-derived sEVs in different type of recipient cells,
9. to determine the utility of *in silico* analyses in the sEV research.

3. Materials and methods

3.1 Cell cultures

5-8F human NPC cell line was kindly provided by Ji Ming Wang (NCI Frederick, MD, USA) and cultured in DMEM supplemented by 10% FBS (Euroclone), 1% MEM non-essential amino acids, 1% MEM vitamin solution and 1% Penicillin-Streptomycin-Amphotericin B mixture (P/S/A; all from Lonza). B16F1 (ECACC 92101203) mouse melanoma cell line was obtained from ECACC and cultured in DMEM supplemented by 10% FBS, 2 mM L-glutamine and 1% P/S/A. For sEV production, both media were prepared using vesicle-depleted FBS.

Primary mouse mesenchymal stem cells (MSCs) were isolated from adipose tissue of 6-8 week old male C57BL/6N mice (Charles River Laboratories), maintained using the MesenCult Expansion Kit (Stemcell Technologies). Mouse embryonic fibroblasts (MEFs; ATCC SCRC-1040) and bEnd.3 mouse endothelial cell line (ATCC CRL-2299) were obtained from ATCC and cultured in DMEM with 15% or 10% FBS and 1% P/S/A. All cell cultures were maintained at 37°C in a humidified incubator with 5% CO_2.

3.2 Ag-TiO_2 photocatalyst particles

For synthesis, commercially available TiO_2 (Degussa P25, Evonik) was used as a standard photocatalyst. Plasmonic Ag nanoparticles were prepared on the surface of TiO_2 in order to enhance the photocatalytic efficiency. Ag-TiO_2 dispersion was made in DPBS at a concentration of 10 mg/ml and sonicated for 30 min directly before adding to the media.

3.3 Stress conditions

5-8F cell cultures were treated at 70% confluency in three different ways: the medium was replaced with (i) fresh medium, (ii) fresh medium supplemented by 0.6 μM doxorubicin, (iii) fresh medium supplemented by light-induced 2.5 μg/ml Ag-TiO_2. During illumination, reactive oxygen species (ROS) are generated on the surface of photocatalyst particles.

In case of B16F1 cell cultures 2 additional culture conditions were applied. One group of cultures was exposed to heat stress by incubating the cells at 42°C for 2 h in every 24 h (a total of 3×). The other group was a control of the Ag-TiO_2 treatment, which was applied to distinguish the effect of illumination itself from the ROS-induced oxidative stress.

Treatment protocols were based on previous optimisation or literature data. In each group, 72 h supernatants of 6 parallel cell cultures were harvested, pooled and subjected to sEV isolation.

3.4 Scanning electron microscopy (SEM)

B16F1 cells seeded to poly-L-lysine-coated 5 mm cover glasses were treated as described above. After 24 h, cells were washed with DPBS and fixed in 2.5% glutaraldehyde with 0.05 M cacodylate for overnight. After washing with DPBS, they were dehydrated with a graded ethanol series, dried with a critical point dryer (Quorum, K850), coated by a 15 nm gold layer (Quorum Q150) and observed under a field-emission scanning electron microscope (Jeol, JSM-7100F/LV). Images were taken in 1,500× and 20,000× magnification.

3.5 sEV isolation and characterisation

Vesicles were isolated by differential filtration and ultracentrifugation. Briefly, supernatants were centrifuged at 780 g for 5 min and at 3,900 g for 15 min at 4°C, then filtered through a 0.22 μm pore-size membrane to remove cells, debris and larger vesicles. Small EVs were pelleted by ultracentrifugation at 150,000 g for 60 min at 4°C. The pellet was washed twice and re-suspended in DPBS. Protein concentrations of B16F1 sEV isolates were measured by the Pierce BCA Protein assay kit (Thermo Scientific) according to the assay protocol. Small EVs were characterised by atomic force microscopy (AFM), dynamic light scattering (DLS) using a Zetasizer Nano S instrument (Malvern Panalytical) and Western blot (WB) assay.

3.5.1 Quantitative comparison of sEV groups

Released number of sEVs was determined by nanoparticle tracking analysis (NTA) using a NanoSight NS500 instrument (Malvern Panalytical) based on the manufacturer's protocol.

3.6 Analysis of the cargo of sEV groups

MiRNomes of sEVs were described for both cell types, and proteomes of sEVs were determined only for B16F1 groups.

3.6.1 miRNA analysis of sEVs

Pellets of sEVs were subjected to miRNA isolation using the NucleoSpin miRNA isolation kit (Macherey-Nagel) according to the manufacturer's instructions. Sequencing was performed on SOLiD 5500xl instrument using SOLiD Total RNA-Seq lit for Small RNA Libraries (Applied Biosystems) based on the manufacturer's protocol. Bioinformatics analysis of raw data was carried out in CLC Genomics Workbench 8.0.2 (Qiagen Bioinformatics) using annotated *Mus musculus* miRNA sequences of the miRBase release 21 as a mapping reference. Only miRNAs with ≥10 read counts were accepted.

3.6.2 LC-MS/MS of B16F1-derived sEVs

Before LC-MS/MS, 25 μg of vesicular proteins were separated by SDS-PAGE and stained with Coomassie blue. Then, each lane was cut to 12 equal bands and subjected to in-gel digestion. The extracted peptides were analysed on an LTQ-Orbitrap Elite (Thermo Scientific) mass spectrometer on-line coupled with a nanoHPLC (nanoAcquity, Waters) system. Searchable peaklists were extracted using Proteome Discoverer 1.4 (Thermo Scientific) and subjected to database search on our in-house Protein Prospector 5.14.1 search engine against the *Mus musculus* and *Bos taurus* protein sequences of the Uniprot database. Proteins were accepted if they was identified with ≥3 unique peptides, but peptides with identical bovine and mouse sequence were excluded. FDR values were less than 1% in all cases.

3.7 Functional comparison of the sEV groups

Bioinformatics analyses were performed on the 5-8F miRNA data and the B16F1 miRNA and protein data, then *in silico* results were verified by *in vitro* assays using the B16F1 sEV isolates.

3.7.1 *In silico* analysis of sEV cargos

Normalised miRNA and protein data were analysed by the Ingenuity Pathway Analysis (IPA, Qiagen Bioinformatics). Using the 'Comparison Analysis' feature, we searched 'Biofunctions' having relevance in NPC or melanoma and $p \leq 0.00001$. Then, some 'Biofunctions' were chosen for further investigation to reveal the regulatory effects of sEVs on them. Using the 'Grow tool', the upstream interacting vesicular molecules were identified for these 'Biofunctions' for each sEV group. Then, using the 'Molecule Activity Predictor (MAP)' tool, we were able to reveal the activation or inhibitory effects of each sEV group for each 'Biofunction'. Figures were edited in the IPA 'Path Designer' and completed with Excel diagrams.

3.7.2 *In vitro* assays for functional comparison of the B16F1 sEV groups

Recipient cells were treated with 200 μg/ml sEV suspensions, or DPBS as a negative control for 24 h, 48 h or 72 h. For longer incubations, treatments were repeated in every 24 h.

3.7.2.1 Ki-67 expression analysis of MSCs

MSCs exposed to sEVs for 24 h and 72 h were fixed in 4% paraformaldehyde (PFA) for 10 min at RT. Then, cells were permeabilised with 0.1% Triton X-100 and non-specific antibody binding was blocked with 5% BSA. We applied direct labelling using anti-mouse/rat Ki-67 monoclonal antibody conjugated to eFluor 615 dye (1:400, eBioScience) in 1.2% BSA

overnight at 4°C. Nuclei were stained with 200 ng/ml DAPI for 15 min at RT. Cells were washed 3× with DPBS for 5 min between each step. Fluorescent images were taken by an Operetta high content imaging system (PerkinElmer) and analysed by an image analysis and machine learning software (SCT Analyzer 1.0). The experiment was repeated 4 times.

3.7.2.2 Cell counting

sEV-exposed MSC cultures in 384-well plates were fixed in 4% PFA for 10 min at RT and stained with 1 µg/ml DAPI for 15 min at RT. Then, the whole area of each well was imaged by a TCS SP8 microscope (Leica) in fluorescent mode, followed by an analysis using the SCT Analyzer 1.0 machine learning software. The experiment was repeated 3 times.

3.7.2.3 Cell cycle analysis

Changes in the cell cycle dynamics of sEV-exposed B16F1 cells were analysed using the Cell-Clock cell cycle assay (Biocolor) according to the assay protocol with 4 repeats.

3.7.2.4 Wound healing assay

Migration of sEV-exposed B16F1 cells and bEnd.3 cells were investigated by scratch assay with 8 and 4 repeats, respectively. Nearly confluent monolayers of cells were wounded by 200 µl pipette tips, washed 3× with medium, then treated with 200 µg/ml sEV suspensions or DPBS in fresh media. Wound closure was followed until the cell-free area decreased below 10% in at least 1 sample; images were taken by an inverted microscope (Zeiss, Axiovert S100) equipped by a Nikon D5000 camera, and analysed the ImageJ software.

3.7.2.5 Analysis of microtissue generation

Equal number of MSC/MEF and B16F1 cells were seeded to 96-well GravityPLUS hanging drop plates (InSphero) in sEV- or DPBS-containing media (5,000 cell/40 µl/well). Microtissue generation was followed for 72 h and imaged by an Axiovert S100 microscope (Zeiss) equipped by a Nikon D5000 camera. Morphological parameters of the microtissues were quantified by the AnaSP software. The experiment was repeated 3 times.

3.8 Statistical analysis

Statistical analyses were performed by the Welch's ANOVA test with Tukey's HSD post-hoc test using a Microsoft Excel add-in, the Real Statistics Resource Pack software. Diagrams were made in GraphPad Prism 5.03. All average values represent mean±SD and number of asterisk denote minimum statistical significance, i.e. *$p<0.05$, **$p<0.01$ and ***$p<0.001$ on figures.

4. Results

In order to study the adaptive responses in the sEV-mediated communication of tumour cells under different microenvironmental conditions, we have investigated stress-induced changes of the 5-8F human NPC- and the B16F1 mouse melanoma cell-derived sEVs.

4.1 Investigation of the NPC-derived sEVs

As a first step, untreated 5-8F cell-released sEVs were isolated by differential filtration and ultracentrifugation and characterised by AFM. Then, 5-8F cell cultures were exposed to cytostatic and oxidative stress as they were treated with 0.6 µM doxorubicin (Doxo) or 2.5 µg/ml light-induced Ag-TiO_2 (Ag-TiO_2), respectively. Untreated cultures were used as a control (Ctrl). After 72 h, sEVs were isolated from the cell culture supernatants, quantified by NTA and subjected to SOLiD sequencing to determine the miRNome of sEV groups. The obtained miRNA data were analysed *in silico* using the IPA software to reveal functional differences between sEV groups.

4.1.1 Descriptive statistics of the NPC-derived sEVs released under different microenvironmental conditions

After the exosomal shape and size was verified by AFM (Fig. 2a), numbers of sEVs were compared across the three sEV groups using Nanosight analysis. We found a significant increase in the sEV production of 5-8F cells, which were exposed to cytostatic (p=0.0146) or oxidative stress (p=0.0006) compared to the Ctrl cultures (Fig. 2b).

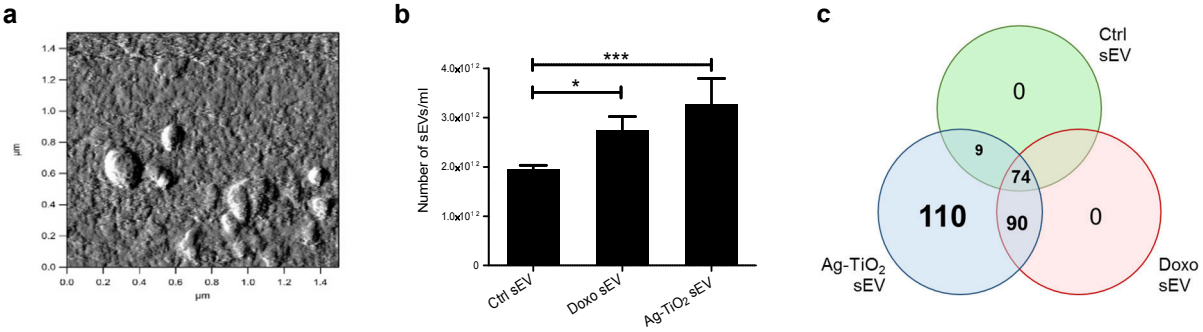

Figure 2. Characterisation of the 5-8F sEVs. (a) High-resolution AFM image of intact sEVs. (b) Number of vesicles in each sEV group quantified by NTA (n=4); each bar represents mean+SD; *p<0.05; ***p<0.001. (c) Comparison of the miRNomes across the three sEV groups.

We also found a substantial increase in the miRNA diversity under both stress conditions. A total of 283 miRNAs were identified by SOLiD sequencing; 26.15% (74 of 283) of these miRNAs were common to each sEV group, 31.80% (90 of 283) were found in both stress sEV groups (but not in Ctrl sEVs), while 38.87% (110 of 283) were exclusively detected in the

Ag-TiO_2 sEVs (Fig. 2c). Ctrl and Doxo sEV-specific miRNAs were not found. In other words, the number of delivered miRNA types increased by 2.22x and 3.82x in the NPC sEVs under cytostatic and oxidative stress, respectively.

4.1.2 *In silico* analysis of functional differences between sEV groups

Since the exosomal cargo is a complex information package containing a large number and wide variety of molecules, it may act on several biological processes in the recipient cells. Here, we aimed to identify these biological processes for all sEV groups. We performed bioinformatics analyses to interpret the biological context of the obtained miRNA data applying the IPA. This software is based on computer algorithms that analyse the functional connectivity of the molecules using the 'Ingenuity Knowledge Base'. For these *in silico* analyses, we set the confidence level to 'Experimentally observed' that enables literature data-based analysis, but not unproven predictions. Phrases between apostrophes are 'IPA-specific terms' throughout the dissertation.

Performing 'Comparison analysis' in the IPA, we identified several NPC-related 'Biofunctions', significantly influenced by any sEV group ($p \leq 0.00001$). This *in silico* analysis revealed, that the sEVs may play a role not only in intracellular and cellular, but in systemic and immunological processes as well.

The 'Grow' tool of IPA enabled to identify the interacting vesicular molecules for selected 'Biofunctions'. Then, the 'MAP' feature of IPA predicted their overall regulatory effects, i.e. activation or inhibitory effects for each sEV group. We found many 'Biofunctions', which can be regulated differently by the sEVs, highlighting the role of the releasing conditions in the vesicular communication of NPC cells.

In general, Ctrl sEVs showed tumour promoting effects; IPA predicted activation of proliferation, viability, migration and EMT, while inhibition of senescence and apoptosis of tumour cells upon exposure to Ctrl sEVs. However, effects of the stress sEV groups on these 'Biofunctions' decreased or turned into the opposite. For instance, activation of cell viability was predicted by less confidence for the Doxo sEVs and changed to inhibition for the Ag-TiO_2 sEVs. The regulation of migration is predicted to switch to inhibitory upon exposure to both stress-exposed cell-derived sEVs. These results suggest that miRNA cargo of NPC-derived sEVs loses its ability to promote tumour progression under stress conditions.

4.2 Investigation of the melanoma-derived sEVs

In the second part of this project, we aimed to investigate the sEV-mediated intercellular communication of stress-exposed B16F1 melanoma cells.

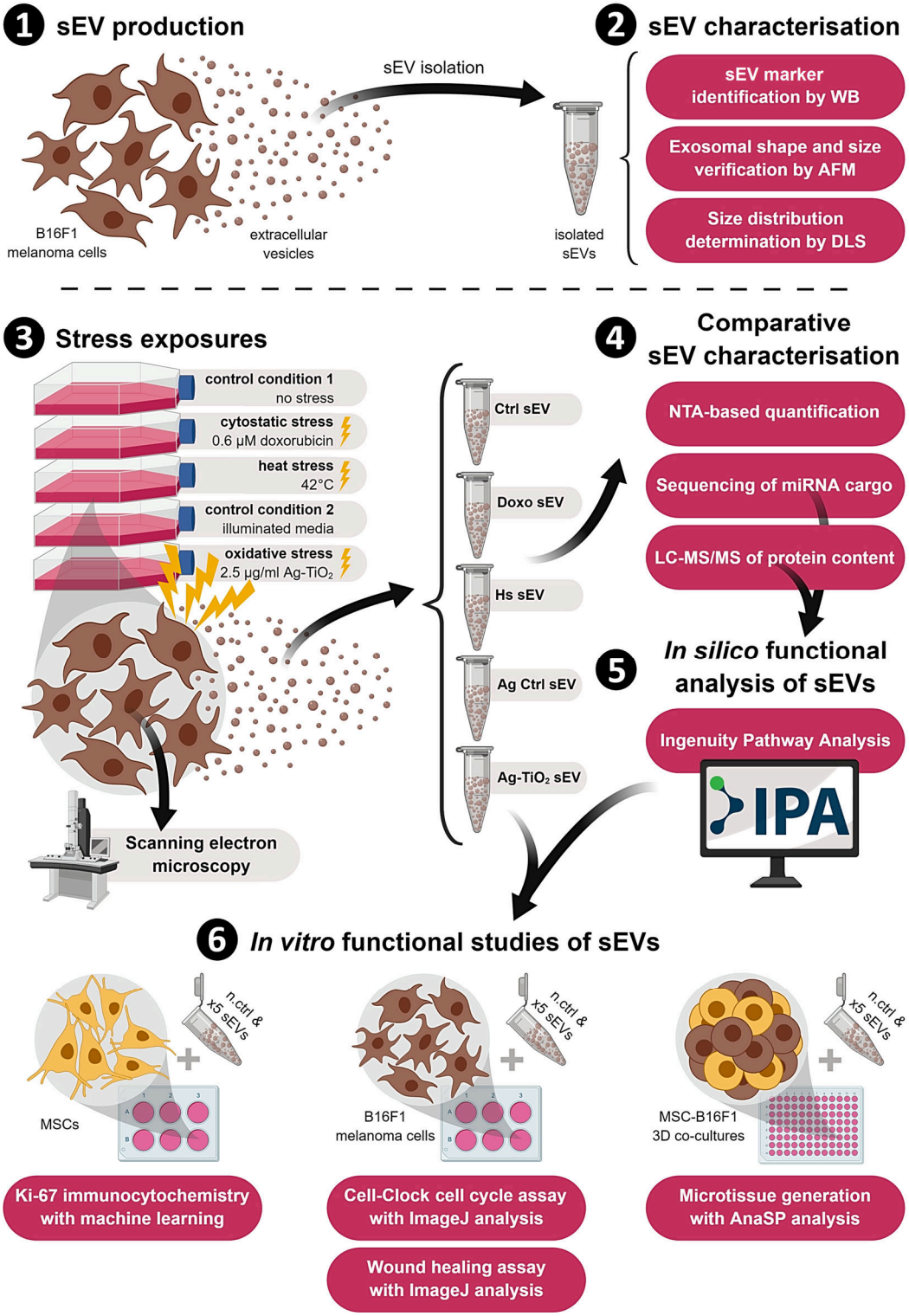

Figure 3. Schematic illustration of the experimental workflow investigating melanoma-derived sEVs. n.ctrl: negative control, x5 sEVs represents the treatments with the 5 sEV groups.

After verification of the exosomal characteristics of the isolated B16F1 sEVs, we investigated their cytostatic, heat and oxidative stress-induced alterations. Melanoma cells were cultured under five different conditions; control cultures (Ctrl) received only culture medium, cytostatic stressed cultures (Doxo) were treated with 0.6 µM doxorubicin, heat stressed cultures (Hs) were incubated at 42°C for 3× 2 h, oxidative stressed cultures (Ag-TiO_2) were treated with 2.5 µg/ml light-induced Ag-TiO_2, and as a control of the oxidative stress (Ag Ctrl), additional cultures were treated with illuminated media. Then, sEV isolates of the five cell culture groups were analysed by NTA, SOLiD sequencing and LC-MS/MS to determine their vesicle number, miRNome and proteome. Functional differences between sEV groups were predicted first, *in silico* using the IPA based on the obtained miRNA and protein data, and then verified by *in vitro* experiments targeting tumour-related cellular functions, such as Ki-67 expression, cell cycle dynamics, migration capacity and microtissue generation of the recipient cells (Fig. 3).

4.2.1 Descriptive statistics of melanoma sEVs released under different microenvironmental conditions

4.2.1.1 Vesicle production of melanoma cells is elevated under suboptimal conditions

SEM revealed spectacular morphological changes of the B16F1 cells in each stressed group (Doxo, Hs and Ag-TiO_2) 24 h after treatments (Fig. 4a). At a 20,000× magnification, we were also able to observe the surface structures of the cells, including exosome-sized vesicles, which were present in higher number on the stressed cells compared to the untreated Ctrl cells (p_{Doxo}=0.00297, p_{Hs}=0.03928, $p_{Ag\text{-}TiO_2}$=n.s., n=5; Fig. 4a,b).

Isolated sEVs were also quantified by the NTA-based NanoSight analysis. There was a significant increase in the vesicle production upon exposure of the donor cells to any stress factors (p_{Doxo}=0.00021, p_{Hs}=0.03006, $p_{Ag\text{-}TiO_2}$=0.02462) compared to the Ctrl cultures (Fig. 4c).

4.2.1.2 Melanoma sEVs may transfer doxorubicin, but not Ag-TiO_2

Using fluorescence spectroscopy, we measured the doxorubicin content of Doxo sEVs, which was less than 10% of the median lethal dose (LD50=100 ng/ml) for mouse melanoma cells, suggesting negligible effects in the recipient cells.

At the same time, encapsulation of Ag-TiO_2 nanoparticles into sEVs was excluded by DLS, chemiluminescence detection and transmission electron microscopy as well.

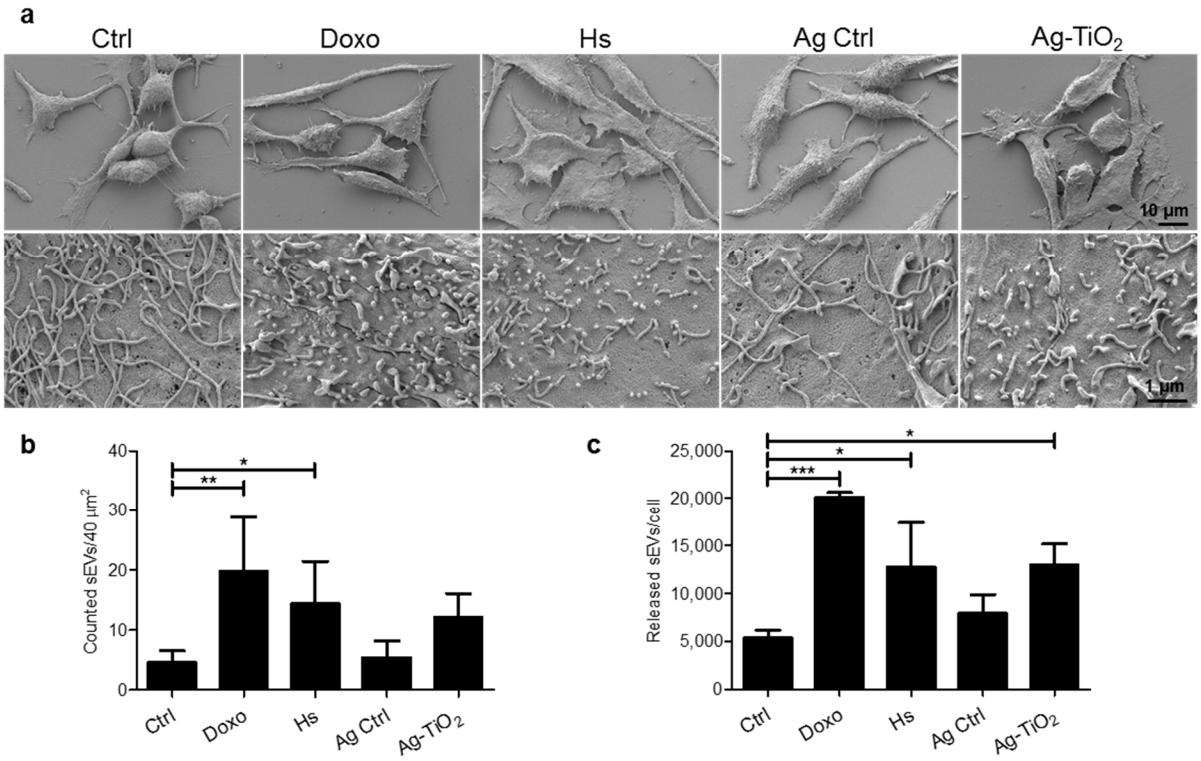

Figure 4. Microenvironmental stress factors resulted in morphological changes and elevated vesicle production of melanoma cells. (a) Scanning electron micrographs of the differently treated melanoma cells. (b) Counted exosome-sized vesicles on the surface of cells using ImageJ (n=5). (c) Number of released vesicles/cell measured by NTA (n=3). Each bar represents mean+SD; *p<0.05, **p<0.01 and ***p<0.001.

4.2.1.3 Molecular pattern of the melanoma sEVs strongly depends on the microenvironmental conditions of the donor cells

To assess the microenvironmental stress-induced alterations of the melanoma sEV cargo, we analysed the miRNA and protein content of the sEV groups by SOLiD sequencing and LC-MS/MS, respectively. As Figure 5 shows, 35.04% (89 of 254) of the detected miRNAs and 59.72% (129 of 216) of the identified proteins were common to all sEV groups. However, the molecular patterns of the five sEV groups showed differences, suggesting that releasing conditions have a critical role in the sEV-mediated communication of melanoma cells (Fig. 5).

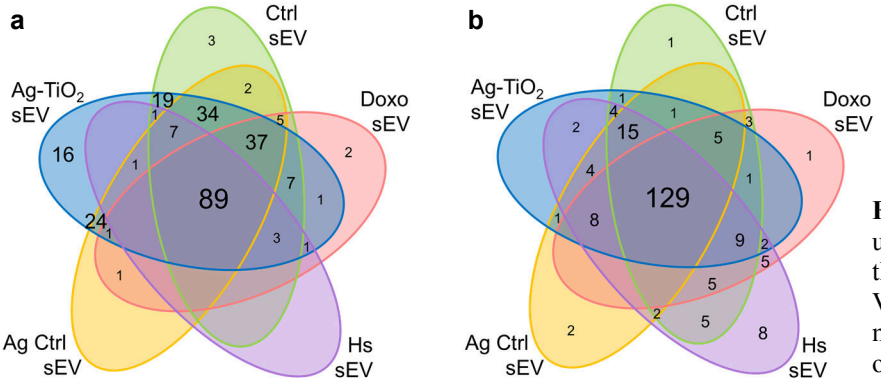

Figure 5. Stress factors caused unique molecular patterns of the melanoma-derived sEVs. Venn diagrams of the (a) miRNomes and (b) proteomes of the five sEV groups.

4.2.2 Comprehensive *in silico* analysis of the functional differences between sEV groups

Bioinformatics analysis was performed to analyse the obtained miRNA and protein data to identify biological processes, which can be influenced by the melanoma sEV groups.

Based on results of the 'Comparison analysis' in the IPA, as in the NPC experiments, we were able to identify several melanoma-related 'Biofunctions', significantly influenced by any sEV group ($p \leq 0.00001$). Among them, we found many intracellular processes, e.g. 'Arrest in G1 phase of tumour cell lines'; cellular processes, e.g. 'Cell movement of melanoma cell lines'; systemic processes, e.g. 'Metastasis of cells' and immunological processes, e.g. 'Activation of leukocytes' as well.

4.2.3 *In silico* predictions-based *in vitro* analyses of the melanoma sEV-induced cellular responses of tumour matrix cells

Focusing on the activation and inhibitory effects, the 'Grow' and 'MAP' features of IPA enabled to identify many 'Biofunctions', which can be regulated differently by the sEVs. Then, *in silico* predicted sEV-induced cellular responses were analysed through *in vitro* methods.

4.2.3.1 Ag-TiO_2 sEVs facilitate proliferation of MSCs

The *in silico* analyses predicted activation of Ki-67 expression for the Ctrl, Hs and Ag-TiO_2 sEVs and 'Proliferation of stem cells' for each sEV groups, suggesting that after internalisation three of the investigated sEV groups may induce Ki-67 upregulation and each of them can promote cell divisions in the recipient stem cells (Fig. 6).

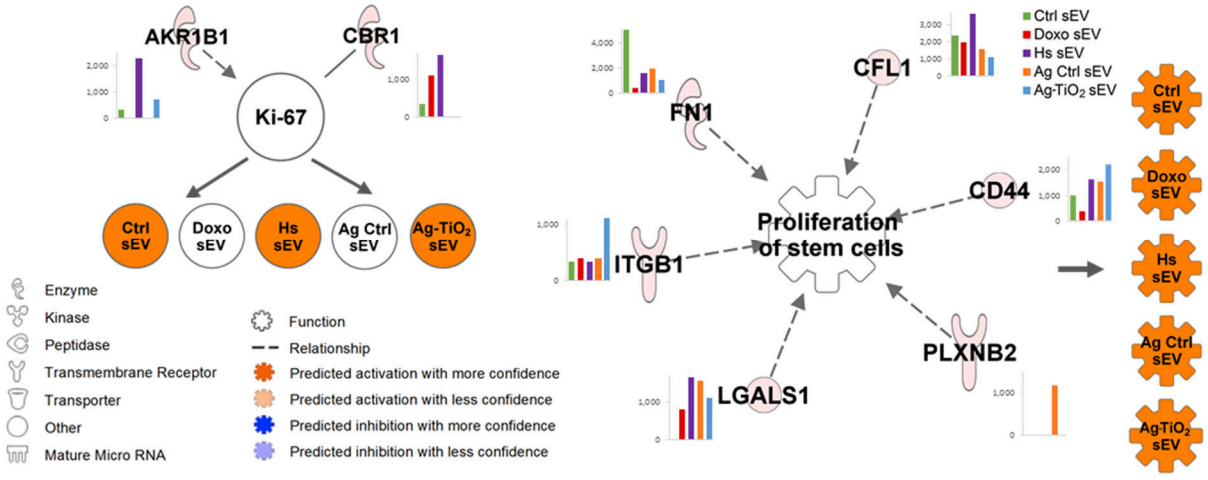

Figure 6. IPA predictions for the regulatory effects of sEV molecules on Ki-67 expression and 'Proliferation of stem cells'. Networks show every upstream regulator proteins accompanied by a bar graph, which represents the normalised expression values of the molecule for each sEV group. Coloured ◌ and ✲ symbols named as the sEV groups display the expected regulation changes of the analysed 'Molecule' and 'Biofunction' upon exposure to the vesicles.

To test the *in silico* predicted differences in the Ki-67 regulation across sEV groups, we treated MSC cultures with 200 µg/ml sEV- or DPBS-containing media as a negative control. After 24 h or 72 h of vesicle exposures, the Ki-67 expression was investigated by immunocyto-chemistry. For the quantitative evaluation of the experiment, the Operetta high-content imaging system and an image analysis and machine learning software (SCT Analyzer 1.0) was applied. Compared to the negative control group, Ag-TiO_2 sEVs significantly increased the proportion of the Ki-67 positive cells after 72 h ($p=0.03572$, $n=4$; Fig. 7a).

Proliferation of MSCs was also tested by direct cell counting using DAPI staining, imaging and machine learning. Proliferation of cells increased upon exposure to Hs and Ag-TiO_2 sEVs as early as 24 h, but different sEVs had distinct influence on this cell function (Fig. 7b).

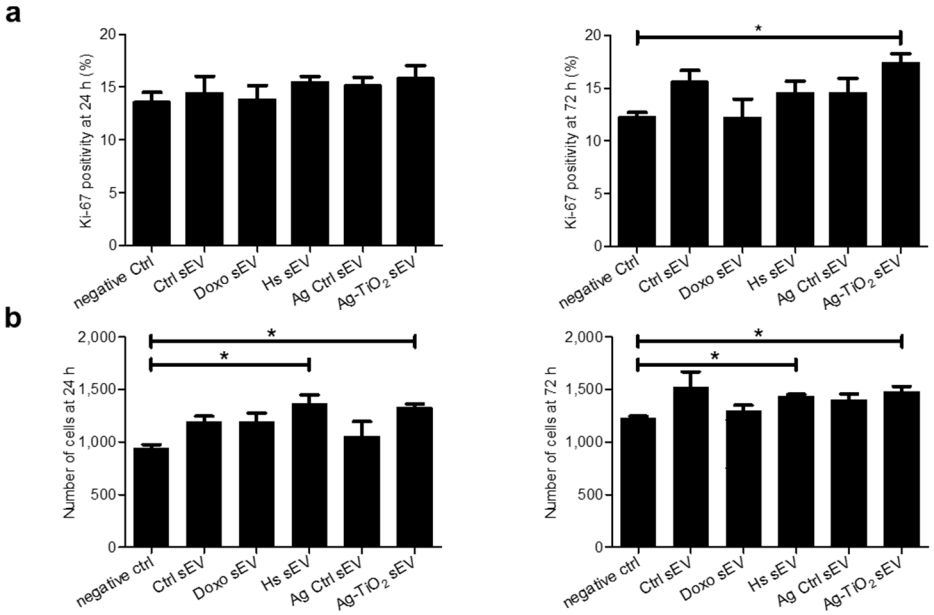

Figure 7. Cell division-related properties of the sEV-exposed MSCs. (a) Percentages of the Ki-67 positive cells 24 h (left panel) and 72 h (right panel) after sEV exposures. (b) Cell numbers of the MSC cultures after 24 h (left panel) and 72 h (right panel) incubation. Bars represent mean+SD, *$p<0.05$ indicates statistical significance.

Our *in vitro* results suggest that melanoma sEVs released under different microenvironmental conditions may have distinct effects on stem cell proliferation. However, beside the IPA predicted interactions, additional molecules and factors, such as the encapsulated doxorubicin, may also be involved in this process.

4.2.3.2 Doxo and Ctrl sEVs affect the cell cycle of tumour cells

IPA analyses predicted inhibition of 'G1 phase of tumour cell lines' and 'G1/S phase transition of tumour cell lines' upon exposure to Ctrl, Doxo and Hs sEVs (Fig. 8). In other words, the molecular content of these vesicles may arrest the recipient tumour cells in the G1 phase.

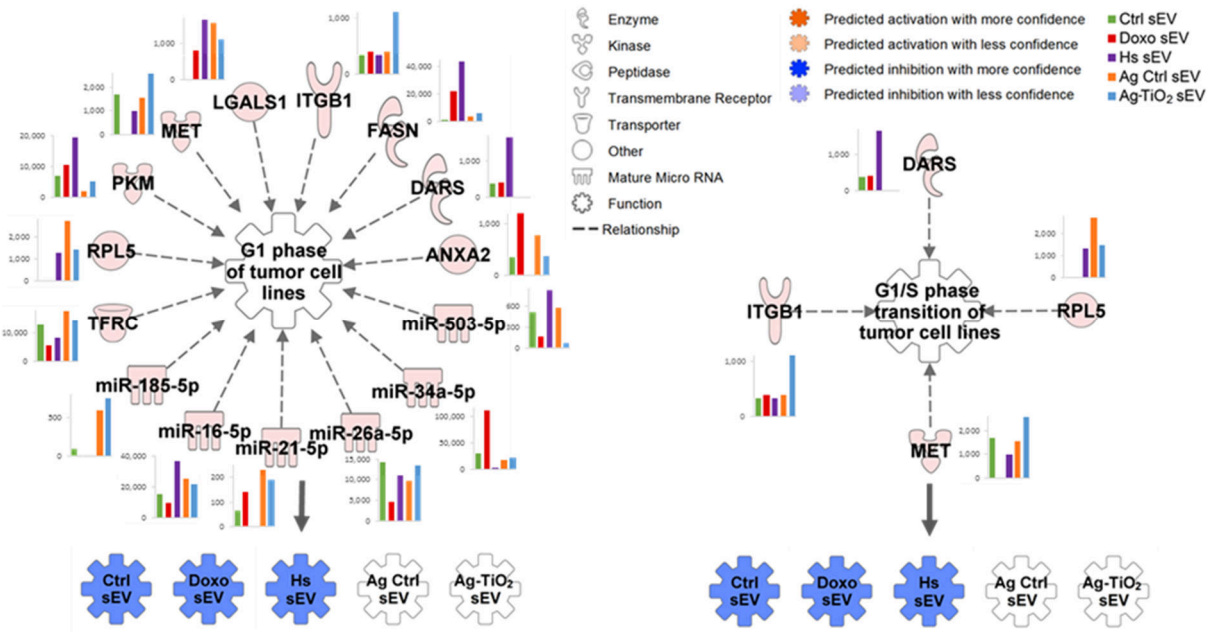

Figure 8. IPA predictions for the regulatory effects of sEV molecules on the 'G1 phase of tumour cell lines' and 'G1/S phase transition of tumour cell lines'. Networks show every upstream regulator proteins and miRNAs accompanied by a bar graph, which represents the normalised expression values of the molecule for each sEV group. Coloured ⚙ symbols named as the sEV groups display the expected regulation changes of the analysed 'Biofunctions' upon exposure to the vesicles.

To test the *in silico* predicted effects of sEVs on tumour cell cycle, we performed Cell-Clock cell cycle assay on B16F1 melanoma cells exposed to sEVs for 24 h, 48 h and 72 h along with a DPBS-treated negative control group. This assay utilizes a vital redox dye that changes colour based on the cell cycle phase. It becomes yellow in G1, green in S/G2 and blue in M phase.

As Figure 9 shows, Ctrl and Doxo sEVs led to an increase in the proportion of the yellow, i.e. G1 phase, cells in a time dependent manner (p_{Ctrl}=0.00346, p_{Doxo}=4.28E-06, n=4). These results confirmed the IPA predicted arrest in the G1 phase by the Ctrl and Doxo, but not by the Hs sEVs, which means, that Ctrl and Doxo sEVs may inhibit the proliferation of tumour cells.

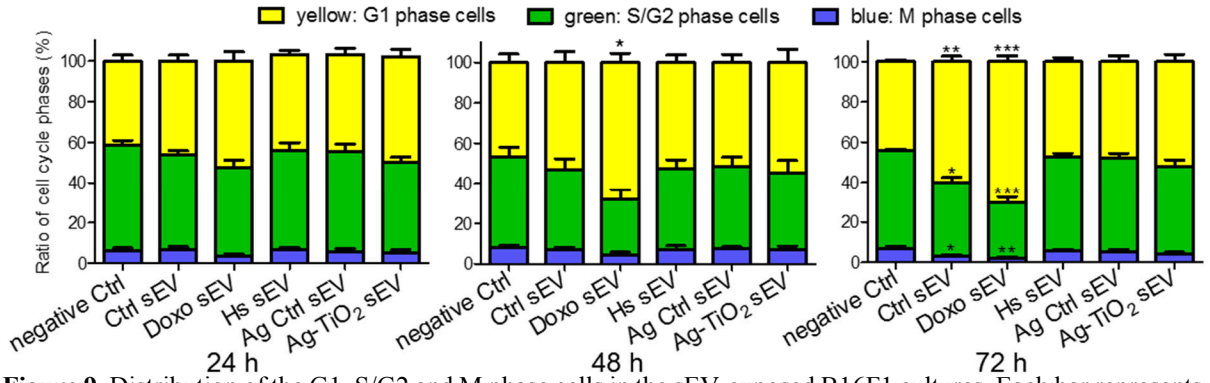

Figure 9. Distribution of the G1, S/G2 and M phase cells in the sEV-exposed B16F1 cultures. Each bar represents mean+SD (n=4), *p<0.05, **p<0.01 and ***p<0.001 indicate statistical significance.

4.2.3.3 sEV-mediated cellular migration depends not only on the type of sEV, but on the recipient cell as well

From many cell movement-related 'Biofunctions', which were predicted to be targeted by sEVs, we chose the 'Migration of melanoma cell lines' and 'Cell migration of endothelial cells' for further IPA and *in vitro* investigations. The *in silico* analyses showed varying sEV effects. More specifically, Doxo and Ag-TiO_2 sEVs are predicted to facilitate the melanoma cell migration, while the three other ones may inhibit this function. At the same time all sEV groups were predicted to enhance the endothelial cell migration (Fig. 10).

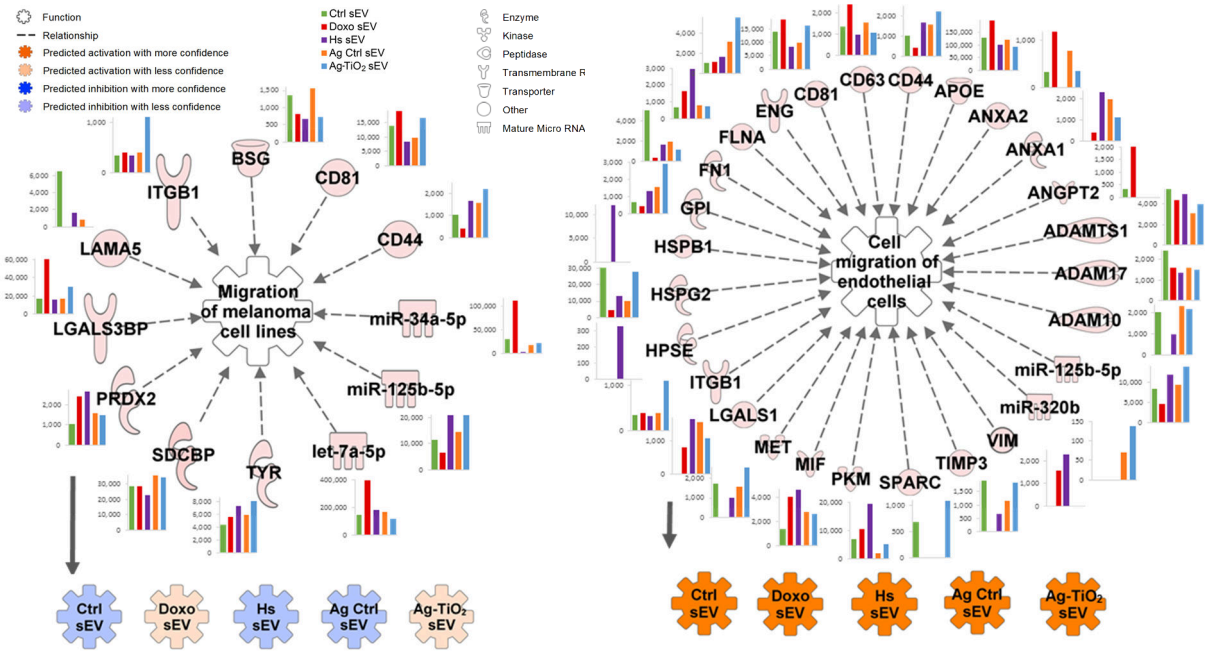

Figure 10. IPA predictions for the regulatory effects of sEV molecules on the (a) 'Migration of melanoma cell lines' and (b) 'Cell migration of endothelial cells'. Network shows every upstream regulator proteins and miRNAs accompanied by a bar graph, which represents the normalised expression values of the molecule for each sEV group. Coloured symbols named as the sEV groups display the expected regulation changes of the analysed 'Biofunction' upon exposure to the vesicles.

Using wound healing assay, we investigated the *in silico* predicted effects of sEVs on migration of B16F1 melanoma and bEnd.3 endothelial cells, which approximated to the IPA-predicted tendency. Migration of melanoma cells into the wounded area was slightly decreased in the presence of Ctrl and Ag Ctrl sEVs, compared to migration of the negative Ctrl cells. Acceleration of wound closure was observed in response to Doxo sEVs (n=8). However, Hs and Ag-TiO_2 sEVs had no effect on tumour cell migration (Fig. 11a). This means that under cytostatic stress, sEVs may convey a message to the neighbouring tumour cells, which enhance their migration.

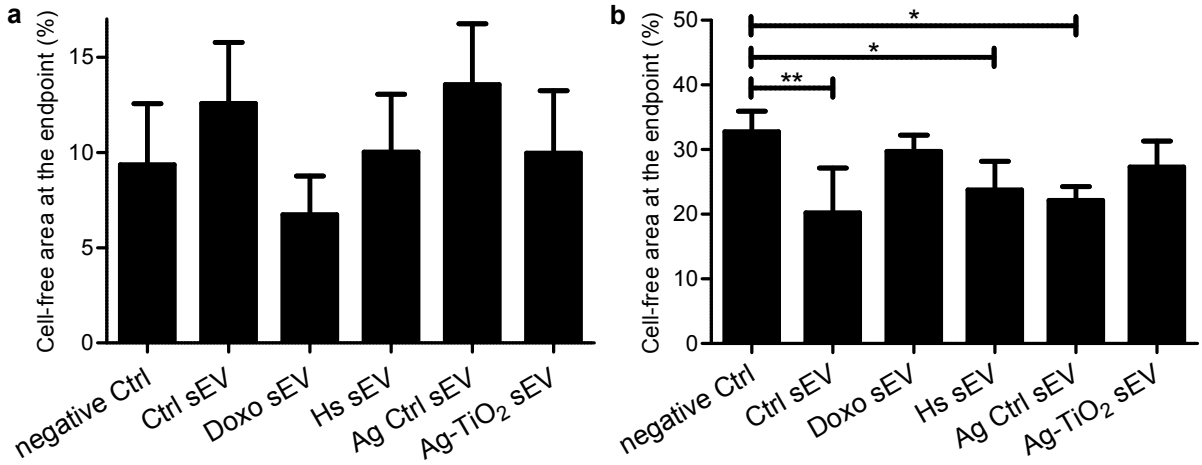

Figure 11. Migration capacity of the sEV-exposed (a) B16F1 and (b) bEnd.3 cell cultures. Bar graphs demonstrate the results of the wound healing assay analysed by the ImageJ wound healing tool. They represent mean+SD values (n_{B16F1}=8, $n_{bEnd.3}$=4), *p<0.05 and **p<0.01 indicate statistical significance.

In case of endothelial cells, Ctrl sEVs showed the highest migration enhancing effect suggesting that released vesicles under normal conditions may promote angiogenesis, but some type of stress conditions may slightly decrease this promoting effects of sEVs (Fig. 11b).

4.2.3.4 Microtissue generation is facilitated independently of the sEV groups

IPA predicted that each of the five sEV groups could activate many 'Biofunctions' related to the formation of a 3D cell interaction matrix, e.g. 'Aggregation of cells' or 'Formation of ECM' (Fig. 12). The intensity of these activations is variable between sEV groups, for example activation of the 'Aggregation of cells' is predicted to be the strongest upon Doxo and Hs sEV exposures.

These *in silico* predictions were also tested *in vitro*. In order to mimic *in vivo* conditions, we established a simplified 3D tumour matrix model co-culturing MSCs or MEFs and B16F1 cells in hanging drop plates. Applying an equal number of the two cell types (a total of 5,000 cells/well), the microtissue generation was followed under sEV exposures and DPBS treatment as a negative control for 72 h. Images of the created microtissues were analysed by the AnaSP software developed for automatic image analysis of multicellular spheroids. Each group of sEVs facilitated the microtissue generation, but Doxo sEVs resulted in the smallest and most compact structures (Fig. 13). This means that surface to volume ratio was higher in the sEV-exposed microtissues, which may enhance the uptake of oxygen, growth factors and nutrients. At the same time, high compactness may reduce the penetration of drugs.

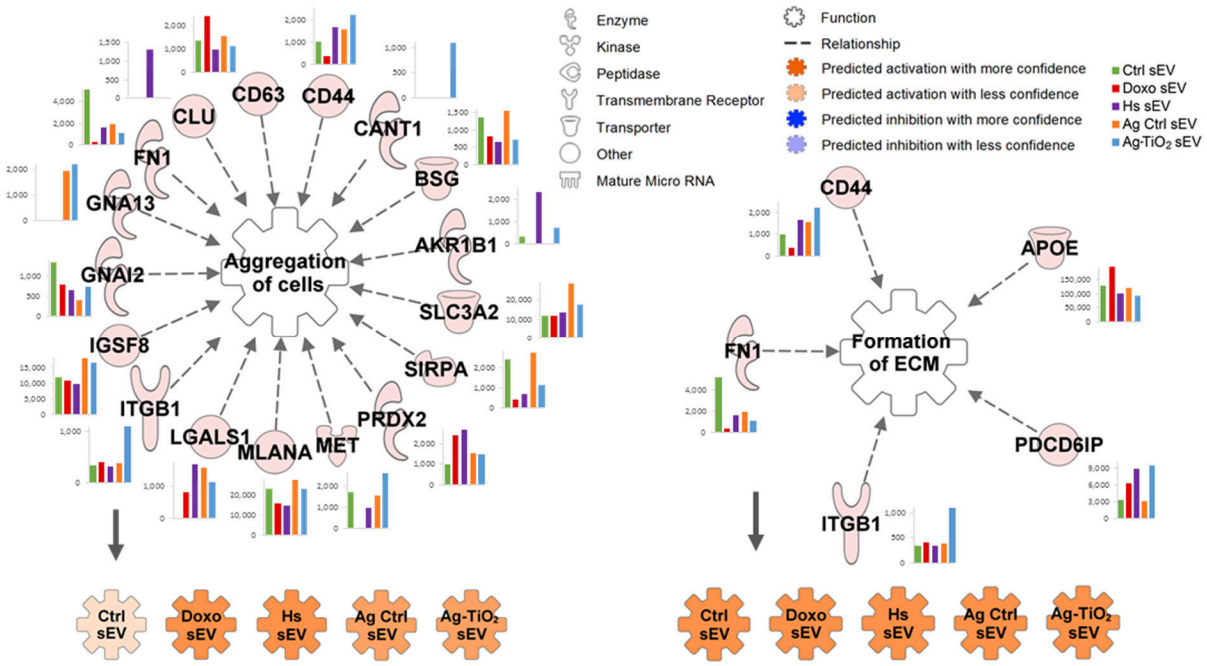

Figure 12. IPA predictions for the regulatory effects of sEV molecules on the 'Aggregation of cells' and the 'Formation of ECM'. Networks show every upstream regulator proteins accompanied by a bar graph, which represents the normalised expression values of the molecule for each sEV group. Coloured symbols named as the sEV groups display the expected regulation changes of the analysed 'Biofunctions' upon exposure to the vesicles.

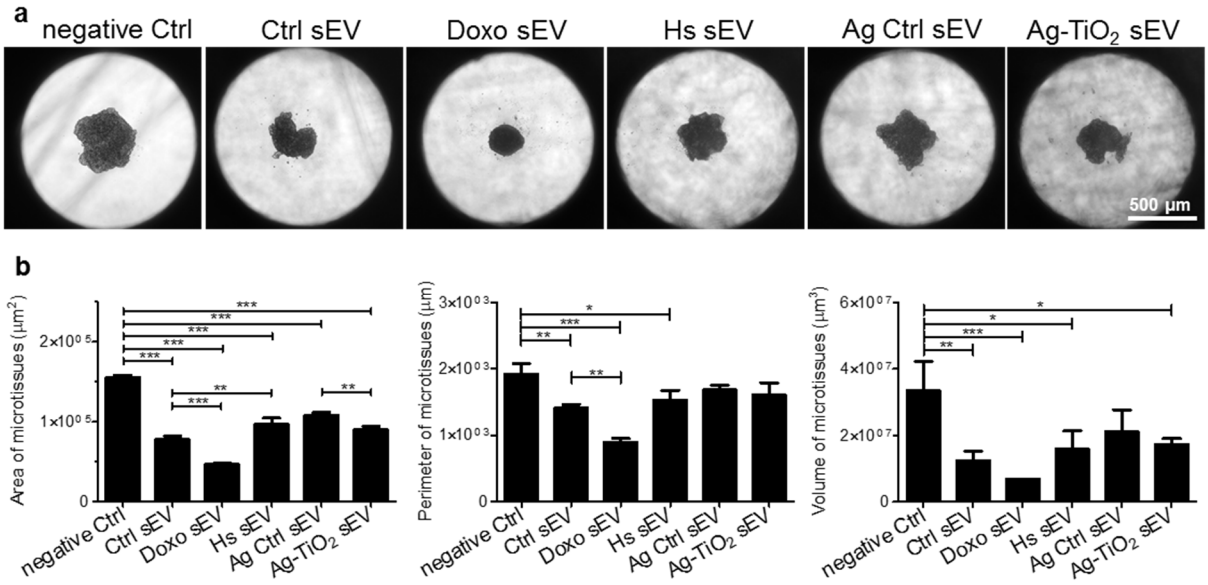

Figure 13. Microtissue generation of MSC-B16F1 co-cultures. (a) Representative images of the generated microtissues after 72 h of sEV exposures. (b) Bar graphs show the area, perimeter and volume statistics of the generated microtissues (mean+SD, n=3). *p<0.05, **p<0.01 and ***p<0.001 indicate statistical significance.

5. Discussion

Several recent papers emphasize the mediating role of exosomes in tumorigenesis, tumour growth, metastasis, angiogenesis, and immune modulation in the tumour macro- and microenvironment. However, effects of the therapy-induced stresses on the vesicular communication of tumour cells have not been elucidated yet. In this study, we investigated effects of the microenvironmental changes on the sEV-mediated communication of tumour cells. We found that cytostatic, heat and oxidative stresses may alter the vesicular cargo, leading to different functional properties of the NPC- and melanoma-derived sEVs in the recipient cells of the tumour matrix.

We showed, that sEVs, being complex information packages may participate in a wide range of signalling pathways. The fact, that a vesicular molecular pattern can influence the cellular homeostasis network at several points, suggests a huge diversity of sEV functions. In conclusion, hundreds of vesicular molecules may have thousands of functional effects in the recipient cells leading to an unconceivable outcome.

Here, we successfully predicted the functional effects of the investigated sEV molecular patterns – induced by five treatment conditions – through bioinformatics analyses using unique combinations of the IPA approaches. Based on our knowledge, our experimental setup was suitable to model the transfer and functional activity of the vesicular cargo in the recipient cells. We demonstrated, that pathway analyses may provide a good approximation to the prediction of the therapy-induced stress responses, suggesting that *in silico* analyses may be useful tools not only in the field of research, but in a clinical setting as well.

This study provides data about the doxorubicin- and Ag-TiO_2-elicited miRNA cargo of the NPC-derived sEVs and a detailed characterisation of the doxorubicin-, heat- and Ag-TiO_2-induced molecular patterns of melanoma-derived sEVs as well. Furthermore, the melanoma sEV-induced response patterns were also characterised in the recipient cells. These results increase our knowledge about the molecular and functional complexity as well as condition-dependent variability of the NPC- and melanoma-derived sEVs. This study contributes to a better understanding of the pathogenesis and therapeutic responses of cancer diseases. It also highlights that indirect effects of any therapy, such as a chemotherapy may have a great influence on the intercellular communication of the affected cells.

Based on this study, we concluded that the molecular pattern of these highly protected information packages is dictated by the microenvironmental conditions, including the therapeutic stress factors. The altered cargo of sEVs is able not only to enhance or suppress existing signalisation pathways, but even trigger *de novo* pathway activations, resulting a unique target cell-specific response pattern in the sEV recipient cells. Recent literature data along with this study suggest that alteration of this complex sEV-mediated intercellular communication of tumour cells deserves special attention among the therapy-induced host responses, which may have a potential influence on the treatment efficacy.

6. New findings

1. Various types of stress conditions increase the sEV production of NPC and melanoma cells at different rates.
2. Number of miRNA types in the NPC sEVs increases by several fold under cytostatic and oxidative stress. Melanoma sEVs also deliver many condition-specific molecules, but miRNA and protein changes show unique patterns for each stress types. Here, we also defined the constant protein cargo of melanoma sEVs.
3. Melanoma cells, similarly to breast carcinoma cells, may transfer doxorubicin by sEVs, but cannot encapsulate Ag-TiO_2 nanoparticles.
4. Transfer and functional activity of the sEV cargo can be modelled *in silico* using the IPA approaches.
5. Different molecular patterns of tumour-derived sEVs, depending on the microenvironmental conditions, may show varying functional properties as well.
6. miRNA content of NPC sEVs promotes tumour progression, but it has inhibitory effects under stress conditions. At the same time, sEV-mediated communication of melanoma cells can adapt to the microenvironmental conditions.
7. Changes in the microenvironmental parameters is reflected in the sEVs-mediated communication of tumour cells through unique response patterns of the recipient cells.
8. The same melanoma sEV population, i.e. the same molecular cargo may induce opposite effects in different types of recipient cells.
9. Our newly developed *in silico* model may predict the sEV-induced effects with a good approximation, which can be useful not only in the research, but in a clinical setting as well.

Acknowledgements

First of all, I would like to express my most sincere gratitude and appreciation to my supervisor, **Krisztina Buzás, PhD** for her guidance, patience and encouragement throughout my PhD studies. I also wish to thank her for introducing me to the world of scientific research and for teaching me to think like a real researcher.

I am grateful to the head of the Institute of Biochemistry and the Laboratory of Image Analysis and Machine Learning in the BRC, **Péter Horváth, PhD** for the scientific and infrastructural support of my project.

I wish to thank my colleagues, **Gabriella Dobra, Edina Gyukity-Sebestyén, Lilla Pintér, Mária Kovács** for the scientific, technical and personal support. Writing this dissertation would not have been possible without their continuous help. I also thank any support for the other members of the Laboratory of Image Analysis and Machine Learning.

I thank all colleagues in the Biological Research Centre, who supported me with constructive ideas or provided laboratory materials or equipment.

I wish to thank all of the **co-authors** of my publications for their contributions to the scientific research. I am grateful to **Filippo Piccinini, PhD** for introducing me to the world of 3D cell cultures.

I also thank the financial support as my research was supported by the GINOP-2.3.2-15-2016-00015; GINOP-2.2.1-15-2017-00052 and NKFI-6-K-11493 and the University of Szeged Open Access Fund.

Finally, I would like to thank my dear, **Zoltán Árpád Váradi** for not only the IT support, but the continuous personal support. I am grateful to my family and relatives, who missed me a lot during the last years.